

## $E_{\text{peak}}$ estimator for Gamma-Ray Bursts Observed by the *Swift* Burst Alert Telescope

T. Sakamoto<sup>1,2,3</sup>, G. Sato<sup>8</sup>, L. Barbier<sup>3</sup>, S. D. Barthelmy<sup>3</sup>, J. R. Cummings<sup>1,2,3</sup>, E. E. Fenimore<sup>5</sup>, N. Gehrels<sup>3</sup>, D. Hullinger<sup>11</sup>, H. A. Krimm<sup>1,7,3</sup>, D. Q. Lamb<sup>9</sup>, C. B. Markwardt<sup>1,6,3</sup>, D. M. Palmer<sup>5</sup>, A. M. Parsons<sup>3</sup>, M. Stamatikos<sup>4,3</sup>, J. Tueller<sup>3</sup>, T. N. Ukwatta<sup>12,3</sup>

### ABSTRACT

We report a correlation based on a spectral simulation study of the prompt emission spectra of gamma-ray bursts (GRBs) detected by the *Swift* Burst Alert Telescope (BAT). The correlation is between the  $E_{\text{peak}}$  energy, which is the peak energy in the  $\nu F_{\nu}$  spectrum, and the photon index ( $\Gamma$ ) derived from a simple power-law model. The  $E_{\text{peak}} - \Gamma$  relation, assuming the typical smoothly broken power-law spectrum of GRBs, is  $\log E_{\text{peak}} = 3.258 - 0.829 \Gamma$  ( $1.3 \leq \Gamma \leq 2.3$ ). We

---

<sup>1</sup>Center for Research and Exploration in Space Science and Technology (CRESST), NASA Goddard Space Flight Center, Greenbelt, MD 20771

<sup>2</sup>Joint Center for Astrophysics, University of Maryland, Baltimore County, 1000 Hilltop Circle, Baltimore, MD 21250

<sup>3</sup>NASA Goddard Space Flight Center, Greenbelt, MD 20771

<sup>4</sup>Oak Ridge Associated Universities, P.O. Box 117, Oak Ridge, Tennessee 37831.

<sup>5</sup>Los Alamos National Laboratory, P.O. Box 1663, Los Alamos, NM, 87545.

<sup>6</sup>Department of Astronomy, University of Maryland, College Park, MD 20742.

<sup>7</sup>Universities Space Research Association, 10211 Wincopin Circle, Suite 500, Columbia, MD 21044.

<sup>8</sup>Institute of Space and Astronautical Science, JAXA, Kanagawa 229-8510, Japan.

<sup>9</sup>Department of Astronomy and Astrophysics, University of Chicago, Chicago, IL, 60637.

<sup>10</sup>Joint Center for Astrophysics, University of Maryland, Baltimore County, 1000 Hilltop Circle, Baltimore, MD 21250

<sup>11</sup>Moxtek, Inc., 452 West 1260 North, Orem, UT 84057

<sup>12</sup>Department of Physics, The George Washington University, Washington, D.C. 20052

take into account not only a range of  $E_{\text{peak}}$  energies and fluences, but also distributions for both the low-energy photon index and the high-energy photon index in the smoothly broken power-law model. The distribution of burst durations in the BAT GRB sample is also included in the simulation. Our correlation is consistent with the index observed by BAT and  $E_{\text{peak}}$  measured by the BAT, and by other GRB instruments. Since about 85% of GRBs observed by the BAT are acceptably fit with the simple power-law model because of the relatively narrow energy range of the BAT, this relationship can be used to estimate  $E_{\text{peak}}$  when it is located within the BAT energy range.

*Subject headings:* gamma rays: bursts

## 1. Introduction

One of the fundamental characteristics of the prompt emission of gamma-ray bursts (GRB) is  $E_{\text{peak}}$ , which is the peak energy in the  $\nu F_{\nu}$  spectrum. According to *BeppoSAX* and *HETE-2* observations,  $E_{\text{peak}}$  for GRBs is widely spread from a few keV to the MeV range as a single distribution (Kippen et al. 2002; Sakamoto et al. 2005). This broad single  $E_{\text{peak}}$  distribution strengthens the argument that these bursts arise from the same origin. Based on this observational evidence, there are several works which try to understand a unified picture of GRBs. For instance, *the off-axis jet model* (Yamazaki et al. 2004; Toma et al. 2005), *the structured jet model* (Rossi et al. 2002; Zhang & Mészáros 2002; Zhang et al. 2004), and *the variable jet opening angle model* (Lamb, Donaghy & Graziani 2005) are the popular unified jet models. On the other hand, there are theoretical models to explain the broad  $E_{\text{peak}}$  distribution in the frame work of the internal shock model (Mészáros et al. 2002; Mochkovitch et al. 2003; Barraud, et al. 2005) and the external shock model (Dermer et al. 1999; Huang et al. 2002; Dermer and Mitman 2003).

There are several important empirical relationships proposed based on the  $E_{\text{peak}}$  energy. One of the most cited relationships is the correlation between  $E_{\text{peak}}$  in the GRB rest frame ( $E_{\text{peak}}^{\text{src}}$ ) and the isotropic radiated energy ( $E_{\text{iso}}$ ), the so called the  $E_{\text{peak}}^{\text{src}}-E_{\text{iso}}$  (Amati) relation (Amati et al. 2002; Amati 2003). Since this relation is extended down to X-ray flashes (Sakamoto et al. 2004, 2006), the dynamic range of this relation is  $\sim 3$  orders of magnitude in  $E_{\text{peak}}^{\text{src}}$  and  $\sim 5$  order of magnitude in  $E_{\text{iso}}$ . The second correlation is between the  $E_{\text{peak}}^{\text{src}}$  energy and the collimation-corrected energy ( $E_{\gamma}$ ), the so called  $E_{\text{peak}}^{\text{src}}-E_{\gamma}$  (Ghirlanda) relation (Ghirlanda et al. 2004). According to Ghirlanda et al. (2004), this relation has much tighter correlation than the  $E_{\text{peak}}^{\text{src}}-E_{\text{iso}}$  relation. Liang & Zhang (2005) investigated a similar relationship, but without using  $E_{\gamma}$  which is heavily dependent on the calculation of

the jet opening angle. They found a good correlation between  $E_{\text{peak}}^{\text{src}}$ ,  $E_{\text{iso}}$ , and the achromatic break time in the afterglow light curve ( $t_{\text{jet}}$ ). The third relationship is between  $E_{\text{peak}}^{\text{src}}$  and the isotropic peak luminosity ( $L_{\text{iso}}^{\text{peak}}$ ), the so called the  $E_{\text{peak}}^{\text{src}}-L_{\text{iso}}^{\text{peak}}$  (Yonetoku) relation (Yonetoku et al. 2004). The latest fourth relationship is between  $L_{\text{iso}}^{\text{peak}}$ ,  $E_{\text{peak}}^{\text{src}}$ , and the time scale of the brightest 45 per cent of the background subtracted counts in the light curve of the prompt emission (Firmani et al. 2006). If these relationships are valid, they must be related to the fundamental physics of GRBs. Thus,  $E_{\text{peak}}^{\text{src}}$  energy provides us fruitful knowledge about the characteristics of the prompt emission of GRBs. Furthermore, knowing the  $E_{\text{peak}}^{\text{obs}}$  energy is crucial to calculating the bolometric fluence which reflects the total radiated energy in the prompt emission.

After the launch of *Swift* (Gehrels et al. 2004) in 2004, the Burst Alert Telescope (BAT; Barthelmy et al. (2005)) has observed about 100 GRBs per year. In about half of the GRBs, the  $E_{\text{peak}}$  energies are very likely to be within the BAT energy range (Sakamoto et al. 2008a). However, due to the relatively narrow energy band of the BAT (15-150 keV in the background subtracted spectrum using the mask modulation), the BAT has a difficulty in determining  $E_{\text{peak}}^{\text{obs}}$ . Our purpose of this study is to find a way to estimate  $E_{\text{peak}}^{\text{obs}}$  when it lies within the BAT energy range.

Here, we report a good correlation between the photon power-law index derived from a simple power-law model and  $E_{\text{peak}}$  based on the spectral simulation study. We use a sample of 31 long BAT GRBs that are well fitted with the power-law times exponential cutoff model, and also 26 GRBs observed by other GRB instruments concurrent with the BAT to confirm our correlation. Our correlation provides an estimate for  $E_{\text{peak}}$  from the photon index in a simple power-law fit at the range from 1.3 to 2.3. We also calculated the  $1\sigma$  confidence level of the estimated  $E_{\text{peak}}$  of our correlation.

## 2. BAT spectral simulation

Because of the systematic difference in the spectral parameters based on the assumption of the spectral model (Band et al. 1993), we decided to perform the simulations for two typical GRB spectral models as input spectra: the smoothly broken power-law model (Band function; Band et al. (1993))<sup>1</sup> and a power-law times exponential cutoff model<sup>2</sup> (CPL) model. We fit the low-energy photon index,  $\alpha$ , and high-energy photon index,  $\beta$ , of 124

---

<sup>1</sup> $dN/dE = K_1 E^{\Gamma_1} \exp[-E(2 + \Gamma_1)/E_{\text{peak}}]$  if  $E < (\Gamma_1 - \Gamma_2)E_{\text{peak}}/(2 + \Gamma_1)$  and  $dN/dE = K_2 E^{\Gamma_2}$  if  $E \geq (\Gamma_1 - \Gamma_2)E_{\text{peak}}/(2 + \Gamma_1)$

<sup>2</sup> $dN/dE \sim E^\alpha \exp(-(2 + \alpha)E/E_{\text{peak}})$

samples of the Band function fit (“BAND” in their notation) in Table 9 of Kaneko et al. (2006) by the normal distribution. We obtained  $\alpha$  of  $-0.87$  with  $\sigma$  of  $0.33$  and  $\beta$  of  $-2.36$  with  $\sigma$  of  $0.31$ . Note that we are not excluding the case of  $\beta > -2$  in our simulations because two reports (e.g., Sato et al. 2005; Kaneko et al. 2006) show fits with  $\beta > -2$  in both time-averaged and time-resolved burst spectra. However, the fraction of simulated spectra with  $\beta > -2$  is only 13% of the total. Similarly, for a CPL model, we fit the low-energy photon index,  $\alpha_{\text{CPL}}$ , for the sample in Table 9 of Kaneko et al. (2006) (“COMP” in their notation; 67 samples) by the normal distribution. We found  $\alpha_{\text{CPL}}$  of  $-1.11$  with  $\sigma$  of  $0.30$  (see Figure 1). These  $\alpha$ ,  $\beta$ , and  $\alpha_{\text{CPL}}$  distributions are used in our spectral simulation.

In our simulations,  $E_{\text{peak}}$  varies from 1.4 keV to 1210 keV in a logarithmic scale. The 15-150 keV fluence varies from  $5 \times 10^{-8}$  to  $5 \times 10^{-5}$  ergs  $\text{cm}^{-2}$  in a logarithmic scale. The fluence range is determined based on the BAT observations (BAT1 catalog; Sakamoto et al. (2008a)). The simulation used 20 values for fluence and 70 values for  $E_{\text{peak}}$ . The exposure time of the spectrum is the best fit log-normal distribution of the BAT  $T_{100}$  duration<sup>3</sup> reported in the BAT1 catalog<sup>4</sup> (See the bottom panel of Figure 1). The normalization of the input spectrum is calculated to be the input fluence value. The spectral simulations are performed 1000 times for each grid point. The background is included in the simulation using the spectrum created from the event data of the false BAT trigger 180931. Since the background is subtracted using the mask modulation, the exposure time of the background spectrum is set as the same as the duration of the foreground spectrum. Four incident angles, on-axis ( $0^\circ$ ),  $15^\circ$ ,  $30^\circ$ , and  $50^\circ$  off-axis, are simulated independently. The simulated spectra are fitted from 14 keV to 150 keV with a simple power-law model<sup>5</sup> (PL), a CPL, and the Band function. Xspec 11.3.2 was used in both creating and fitting the simulated spectra.

Figure 2 shows the numbers of the simulated spectra which have  $\Delta\chi^2$  ( $\Delta\chi^2 \equiv \chi_{\text{PL}}^2 - \chi_{\text{Band}}^2$  for the Band function or  $\Delta\chi^2 \equiv \chi_{\text{PL}}^2 - \chi_{\text{CPL}}^2$  for a CPL model) greater than 6<sup>6</sup> as a function of the  $E_{\text{peak}}$  and the energy flux in the 15-150 keV band. This  $\Delta\chi^2 > 6$  corresponds to  $>2.4 \sigma$  confidence. The figures in the left and right row show the results based on the Band function and a CPL model, respectively. We note the distinct differences in the shapes of the confidence contours, especially at low  $E_{\text{peak}}$ , between the Band function and a CPL model as an input spectrum. The results show that if a CPL model is indeed a true

---

<sup>3</sup>The duration includes from 0 to 100% of the GRB fluence.

<sup>4</sup>The duration between tstart and tstop time of the fluence table.

<sup>5</sup> $dN/dE \sim E^{-\Gamma}$

<sup>6</sup>This is a current criterion used in the BAT team for reporting the spectral parameters based on a CPL fit in the BAT refined circular of the Gamma-ray Burst Coordinates Network.

spectral shape, BAT can measure  $E_{\text{peak}}$  at the lower boundary of its energy range ( $\sim 15$  keV) with a very high significance. On the other hand, a low  $E_{\text{peak}}$  measurement would be very challenging if the Band function is the true spectral shape. Figure 3 explains the reason for these differences. The figure shows the calculated photon spectra in a CPL model and the Band function for  $E_{\text{peak}} = 15$  keV. In a CPL model, the spectrum can not be fit with a PL model because of the curved shape (exponential component) in the BAT observed energy band. Therefore, we would expect a significant improvement in  $\chi^2$  with a CPL fit over a PL fit. However, in the Band function, due to the extra power-law component (high energy power-law component) in the formula, the spectrum at the BAT observed energy band would be just a simple power-law with a high energy photon index. This is the reason why we see a difference in the confidence contours based on the assumed spectral models. The results also show that the  $E_{\text{peak}}$  measurement becomes difficult for BAT when  $E_{\text{peak}}$  is below 30 keV or above 100 keV in the Band function shape. In the CPL shape,  $E_{\text{peak}}$  can be determined even at  $\sim 15$  keV.

Figure 4 shows the number of the BAT GRBs which can be acceptably fit by a PL model and by a CPL model as a function of the 15-150 keV fluence. The data are from the BAT1 catalog. In the case of an incident angle less than 25 degrees, a CPL model becomes an acceptable fit for fluence  $>10^{-6}$  ergs  $\text{cm}^{-2}$ . However, a PL model still be acceptable fit if  $E_{\text{peak}}$  is located above or below the BAT energy range. On the other hand, the fluence must typically be greater than  $3 \times 10^{-6}$  ergs  $\text{cm}^{-2}$  in the case of an incident angle greater than 50 degrees. These threshold fluences required to measure  $E_{\text{peak}}$  in the BAT data correspond to the  $\sim 50\%$  confidence contour (green) in our simulation results of Figure 2.

Next, we made histograms of  $E_{\text{peak}}$  for each photon index on a 0.1 grid from 0 to 3.5 using the range of fluences corresponding to the  $1-\sigma$  interval of the BAT observed fluence distribution in the BAT1 catalog. The  $1-\sigma$  fluence interval corresponds to the range from  $3.4 \times 10^{-7}$  ergs  $\text{cm}^{-2}$  to  $5.4 \times 10^{-6}$  ergs  $\text{cm}^{-2}$ . This selection of the fluence range allows us to reduce the systematic effect of the inclusion of unrealistically bright or dim simulations. Furthermore, since we are interested in estimating the  $E_{\text{peak}}$  for the bursts which do not show a significant improvement in  $\chi^2$  by a CPL fit over a PL fit, we also only selected the simulated spectra with  $\Delta\chi^2 = \chi_{\text{PL}}^2 - \chi_{\text{CPL}}^2 < 6$ . Because the numbers of simulated spectra are different for each  $E_{\text{peak}}$  grid due to these selections, we normalized the number of simulated spectra in each  $\Gamma$ - $E_{\text{peak}}$  grid by the total number of spectra in each  $E_{\text{peak}}$  grid. Figure 5 shows the contour map of the photon index ( $\Gamma$ ) and  $\log E_{\text{peak}}$  for the Band function (left) and a CPL (right) model. There is a correlation between  $\Gamma$  and  $\log E_{\text{peak}}$  in the range from 1.3 to 2.3 of  $\Gamma$  for the Band function. The correlation continues to  $\Gamma = 3.0$  in the case of a CPL model for the same reason as we demonstrated in Figure 3. It might be interesting to note that a very steep photon index such as  $\Gamma \sim 3$  is not possible to achieve if the source

spectrum is the Band function. In this case, the source spectrum might be much closer to a CPL shape. One important conclusion is that the correlation between  $\log E_{\text{peak}}$  and  $\Gamma$  exists independent of the incident angle of the burst. Therefore, this correlation, the  $E_{\text{peak}}$  -  $\Gamma$  relation, can be used for all BAT long GRBs within the allowed  $\Gamma$  range, although with larger uncertainty for GRBs at large incidence angle.

We extracted the peak  $E_{\text{peak}}$  value from each histogram of  $\Gamma$  and fit with a linear function using the range from  $1.3 < \Gamma < 2.3$  for both the Band function and a CPL model. Although the correlation exists until  $\Gamma = 3$  in a CPL case, we use the same  $\Gamma$  range for the Band function and a CPL model to investigate the systematic difference based on the assumption of the source spectrum. The best fit  $E_{\text{peak}}$ - $\Gamma$  relations are summarized in Table 1 (Band function) and Table 2 (CPL). To estimate the  $1-\sigma$  uncertainty of the relation, we found 16% and 84% points of  $E_{\text{peak}}$  from each histogram of  $\Gamma$  and fitted with a cubic function from  $1.3 < \Gamma < 2.3$ . The best fit cubic functions of the lower and higher  $1-\sigma$  confidence level are also summarized in Table 1 and Table 2. Figure 6 shows the best fit functions of the  $E_{\text{peak}}$  -  $\Gamma$  relation and its  $1-\sigma$  confidence level with the data points used in the fittings. We note that the wide  $E_{\text{peak}}$  range in the simulations (in our case from 1.4 keV to 1210 keV) is essential to derive the  $1-\sigma$  confidence level of the relation. If the  $E_{\text{peak}}$  range in the simulations is not wide enough such as from 10 keV to 500 keV, we noticed that the confidence level will be underestimated by a factor of 2 for the upper limit at  $\Gamma$  of 1.3 and by a factor of 5 for the lower limit at  $\Gamma$  of 2.0. Due to the smoothly curved shapes of the Band function and the CPL model, the  $E_{\text{peak}}$  grids in the simulations have to be an order of magnitude wider than the energy range of the instrument, so that a curvature (or  $E_{\text{peak}}$ ) in the spectrum is completely outside the energy range of the instrument for the  $E_{\text{peak}}$  around the energy limits of the instrument. However, we also notice that the best fit  $E_{\text{peak}}$  -  $\Gamma$  relation itself is less sensitive to the energy limits on the simulations. Although the confidence level is different between the Band function and a CPL model, the best fit linear function shows little difference between these two spectral models. We also calculated the relation weighting the results at the incident angles of  $0^\circ$ ,  $15^\circ$ ,  $30^\circ$ , and  $50^\circ$  by the distribution of the incident angle of the BAT GRBs (Figure 7). Hereafter, we call this relation as the weighted  $E_{\text{peak}}$  -  $\Gamma$  relation. The contour plots of the weighted  $E_{\text{peak}}$  -  $\Gamma$  relation, the plot of the best fit functions, and the formula of the best fit functions are shown and summarized in Figure 8, Figure 9, and Table 1 and Table 2, respectively.

In the application of our  $E_{\text{peak}}$  -  $\Gamma$  relation, we strongly encourage the reader to use the result based on the Band function as a prior. The main reason for also performing the simulations of a CPL model as a prior is to see the systematic effect due to a prior assumption of the spectral model. Our results are clearly demonstrating the effect of the assumed spectral model. From the various measurements of the burst spectra by different

instruments, the true burst spectrum is very likely to be the Band function at least for long GRBs. Therefore, the  $E_{\text{peak}} - \Gamma$  relation based on the Band function as a prior is the most suitable relation to apply for the BAT long GRBs.

### 3. Comparison to other $E_{\text{peak}}$ Measurements

To investigate the validity of our simulation study, we used the spectral parameters on the BAT1 catalog (Sakamoto et al. 2008a). Table 3 shows the spectral parameters of 31 long GRBs ( $T_{90} > 2$  seconds) having  $\Delta\chi^2$  of greater than 6 in a CPL model over a PL model fit. Figure 10 shows  $E_{\text{peak}}$  energy in a CPL model and the photon index,  $\Gamma$ , in a PL model for the BAT GRBs overlaid with the weighted  $E_{\text{peak}} - \Gamma$  relation. We also plot  $\Gamma$  derived from the BAT data and  $E_{\text{peak}}$  reported by Konus-Wind or *HETE-2* in the Gamma ray bursts Coordinates Network (GCN) listed in table 4. As seen in the figure, the  $1-\sigma$  confidence level of the  $E_{\text{peak}} - \Gamma$  relation based on the simulation study is consistent with the 90% confidence level of  $\Gamma$  observed by the BAT and  $E_{\text{peak}}$  observed by the GRB instruments. However, we want to caution about using our  $E_{\text{peak}} - \Gamma$  relation for estimating  $E_{\text{peak}}$ . Our estimator is based on prior assumptions of the low-energy and/or the high-energy photon index measured by the BATSE. Therefore,  $E_{\text{peak}}$  based on our  $E_{\text{peak}} - \Gamma$  relation only provides a likelihood of the  $E_{\text{peak}}$  value not the “measurement.”

The calculation of the bolometric flux or fluence is another challenge when using the BAT data alone. However, since the low energy photon index  $\alpha$  and the high energy photon index  $\beta$  of the Band function are quite stable parameters even if  $E_{\text{peak}}$  varies from a few keV to a few MeV (e.g., Sakamoto et al. 2005; Kaneko et al. 2006), one could estimate the bolometric flux or fluence assuming the best fit  $\alpha$  and  $\beta$  from the BATSE time-averaged spectral analysis of Kaneko et al. (2006), and applying the best fit  $E_{\text{peak}}$  derived from our  $E_{\text{peak}} - \Gamma$  relation. To get the normalization for the Band function spectrum, one would scale the Band spectrum so that the flux in the BAT energy range matches to the BAT measured flux. One can also estimate the error of the flux or fluence by propagating the errors of  $\alpha$ ,  $\beta$ ,  $E_{\text{peak}}$ , and the normalization, however this estimate will not be strictly correct because the parameters of the Band function are correlated. Finally, we caution against relying too heavily on this derived bolometric flux or fluence, since the method described uses averaged  $\alpha$  and  $\beta$  from a different burst population and an estimated, rather than measured  $E_{\text{peak}}$ .

#### 4. Discussion

According to Sakamoto et al. (2005), an equal number of X-ray flashes (XRF), X-ray-rich GRBs (XRR), and GRBs are reported in the HETE-2 GRB sample. Their classification of GRBs based on the fluence ratio between the 2-30 keV and 30-400 keV bands is almost the equivalent of classifying GRBs by  $E_{\text{peak}}$ . The boundaries of  $E_{\text{peak}}$  between an XRF and an XRR, and an XRR and a GRB are around 30 keV and 100 keV. When we use the weighted  $E_{\text{peak}} - \Gamma$  relation for the Band function to calculate the corresponding  $\Gamma$  for each  $E_{\text{peak}}$ ,  $\Gamma$  is  $\sim 2.2$  and  $\sim 1.5$  for  $E_{\text{peak}}$  of 30 keV and 100 keV, respectively. Applying these  $\Gamma$  criteria to a sample of 206 BAT GRBs, excluding short GRBs ( $T_{90} < 2$  seconds) and GRBs with incomplete dataset, we found that the number of XRFs, XRRs, and GRBs are 20, 126, and 60 respectively. The numbers of XRFs, XRRs, and GRBs in the HETE-2 sample are 16, 19, and 10 respectively. Therefore, the ratio of the numbers of XRRs and GRBs is identical for both BAT and HETE-2 sample. The small numbers of XRFs in the BAT sample is due to the difficulty in observing very soft XRFs in the BAT (Band 2003, 2006). However, as mentioned in Band (2006), it is very difficult to determine the actual detection threshold of the BAT due to its complexity in the triggering algorithm. Although nothing could be addressed about the actual number of XRFs, the number of GRBs in XRRs and GRBs seen in the BAT sample is consistent with the HETE-2 sample. The detailed study of the Swift XRFs and XRRs is presented elsewhere (Sakamoto et al. 2008b).

Butler et al. (2007) calculated  $E_{\text{peak}}$  by their Bayesian approach for 218 *Swift* GRBs using only the BAT data. Based on their calculated  $E_{\text{peak}}$  and the bolometric fluence, they claimed that all of the empirical relations,  $E_{\text{peak}}^{\text{src}} - E_{\text{iso}}$  (Amati et al. 2002),  $E_{\text{peak}}^{\text{src}} - L_{\text{iso}}^{\text{peak}}$  (Yonetoku et al. 2004), and  $E_{\text{peak}}^{\text{src}} T_{45} - L_{\text{iso}}^{\text{peak}}$  (Firmani et al. 2006), proposed in the pre-*Swift* observations are not valid for the *Swift* BAT sample. We investigated the validity of their  $E_{\text{peak}}$  by checking  $E_{\text{peak}}$  obtained by using our  $E_{\text{peak}} - \Gamma$  relation. We created the BAT spectra for their GRB samples by the time interval reported on Table 1 of Butler et al. (2007). Then, we fit the spectrum by a PL model to extract the best fit  $\Gamma$ . By only selecting their  $\Gamma$  within the allowed  $\Gamma$  range for applying our  $E_{\text{peak}} - \Gamma$  relation ( $1.3 < \Gamma < 2.3$ ) and also excluding the short GRBs (156 samples in total), we calculated  $E_{\text{peak}}$  applying our weighted  $E_{\text{peak}} - \Gamma$  relation for the Band function. Figure 11 shows the  $E_{\text{peak}}$  reported on Butler et al. (2007) versus  $E_{\text{peak}}$  derived from our weighted  $E_{\text{peak}} - \Gamma$  relation for the Band function. Although the error bars are large in both estimators, the figure shows that  $E_{\text{peak}}$  of the Butler et al. (2007) sample has a systematically higher  $E_{\text{peak}}$  compared to that from our  $E_{\text{peak}} - \Gamma$  relation. About 20% of the Butler et al. (2007) sample selected based on the range of  $\Gamma$  from 1.3 to 2.3 exceeds  $E_{\text{peak}} \sim 150$  keV which is the limit of the estimated  $E_{\text{peak}}$  using our  $E_{\text{peak}} - \Gamma$  relation for  $\Gamma = 1.3$ . Furthermore, we are already excluding 20% of the Butler et al. (2007) sample because those bursts fall outside limit range of  $\Gamma$  from 1.3 to 2.3 in our relation. This

limit is determined because  $E_{\text{peak}}$  is very likely located outside of the BAT energy range, and therefore, the BAT data alone can not constrain about  $E_{\text{peak}}$  (the BAT data only can provide the limit in  $E_{\text{peak}}$ ). In total, about 35% of the Butler et al. (2007) samples are obviously inconsistent with the  $E_{\text{peak}}$  estimated based on our  $E_{\text{peak}} - \Gamma$  relation. However,  $E_{\text{peak}}$  is *constrained* in the most of the Butler et al. (2007) sample. These results provide a caution for the method for estimating  $E_{\text{peak}}$  in Butler et al. (2007).

Butler et al. (2007) justify their *Swift*-only  $E_{\text{peak}}$  estimates in part by comparing to *Konus-Wind* measurements of  $E_{\text{peak}}$  for the same bursts. They also using the  $E_{\text{peak}}$  distribution as a prior. However, the assumption of  $E_{\text{peak}}$  measured by *Konus-Wind* should be identical to that of BAT in Butler et al. (2007) might not be valid. Because BAT has a significantly larger effective area and also relatively softer energy band than *Konus-Wind*, the time interval for creating the time-averaged spectrum based on the BAT data could be systematically longer than that of *Konus-Wind* (Sakamoto et al. in preparation). This longer time interval for the time-averaged spectrum in BAT might lead to a systematically lower  $E_{\text{peak}}$  which might contradict with the  $E_{\text{peak}}$  based on the *Konus-Wind* data alone. For instance, GRB 060117, which has individual measurements of  $E_{\text{peak}}$  from the BAT and the *Konus-Wind* data (see Table 2 and Table 3), shows a smaller  $E_{\text{peak}}$  in the BAT data. The duration reported based on the *Konus-Wind* data is  $\sim 20$  seconds (Golenetskii et al. 2006b). On the other hand, the duration used to accumulate the BAT spectrum is  $\sim 30$  seconds (Sakamoto et al. 2008a). We confirmed based on our cross-calibration work that there is no systematic difference in  $E_{\text{peak}}$  of this burst between BAT and *Konus-Wind* if we select exactly the same time interval for accumulating the spectrum (Sakamoto et al. in preparation). Therefore, we believe that a prior assumption of  $E_{\text{peak}}$  based on a particular GRB instrument might introduce an another level of a systematic error in the analysis. Most importantly, we believe that testing these empirical relations, which require the broad-band spectral properties of the prompt GRB emission, by using only the BAT narrow-band data could lead to a wrong conclusion. Current on-going activity for analyzing the spectral data of simultaneously observed BAT GRBs by other GRB missions such as *Konus-Wind* and *Suzaku*/WAM (Sakamoto et al. in preparation; Krimm et al. in preparation) is indeed a necessary step to answer for the validation of these empirical relations. We might want to emphasize that the  $1-\sigma$  confidence level of our  $E_{\text{peak}} - \Gamma$  relation based on the Band function includes most of  $E_{\text{peak}}$  reported by other instruments (see Figure 10). Therefore, the confidence level which we are quoting in our estimator is large enough to include the systematic problem in  $E_{\text{peak}}$  among the different instruments.

We report the correlation between  $E_{\text{peak}}$  and the photon index,  $\Gamma$ , of the BAT prompt emission spectrum based on our simulation study. Using this relation, it is possible to estimate  $E_{\text{peak}}$  from  $\Gamma$  in the range from 1.3 to 2.3. We also performed the spectral simulations

for assuming various incident angles ( $0^\circ$ ,  $15^\circ$ ,  $30^\circ$  and  $50^\circ$ ) and different spectral models (Band function and CPL). However, none of these systematic effects changes the relation. In the application, the  $E_{\text{peak}} - \Gamma$  relation based on the Band function as a prior is the appropriate formula to use. The  $E_{\text{peak}} - \Gamma$  relation could be informative for classifying the BAT GRBs from the photon index alone as derived from a simple power-law model which is the best fit for about 80 % of the whole population of the BAT GRBs.

We would like to thank the anonymous referee for comments and suggestions that materially improved the paper.

## REFERENCES

- Amati, L., et al. 2002, *A&A*, 390, 81
- Amati, L., 2003, *ChJAA*, Vol. 3, Supplement, pp. 455-460
- Barthelmy, S.D., et al. 2005, *Space Sci. Rev.*, 120, 143
- Band, D. L., et al. 1993, *ApJ*, 413, 281
- Band, D. L., 2003, *ApJ*, 588, 945
- Band, D. L., 2006, *ApJ*, 664, 378
- Barraud, C., Daigne, F., Mochkovitch, R., Atteia, J. L. 2005, *A&A*, 440, 809
- Butler, N.R., Kocevski, D., Bloom, J.S., Curtis, J.L. 2007, *ApJ*, 671, 656
- Crew, G., et al. 2005a, GCN Circ. 3890, <http://gcn.gsfc.nasa.gov/gcn3/3890.gcn3>
- Crew, G., et al. 2005b, GCN Circ. 4021, <http://gcn.gsfc.nasa.gov/gcn3/4021.gcn3>
- Dermer, C. D., Chiang, J., and Böttcher 1999, *ApJ*, 513, 656
- Dermer, C. D., and Mitman, K. E. 2003, in ASP Conf. Ser. 312, Third Rome Workshop on Gamma-Ray Bursts in the Afterglow Era, ed. M. Feroci et al. (San Francisco: ASP), 301
- Firmani, C, Ghisellini, G., Avila-Reese, V., and Ghirlanda, G. 2006, *MNRAS*, 370, 185
- Gehrels, N., et al. 2004, *ApJ*, 611, 1005

Ghirlanda, G., Ghisellini, G., Lazzati, D., 2004, *ApJ*, 616, 331

Golenetskii, S., et al. 2005a, *GCN Circ.* 3152, <http://gcn.gsfc.nasa.gov/gcn3/3152.gcn3>

Golenetskii, S., et al. 2005b, *GCN Circ.* 3474, <http://gcn.gsfc.nasa.gov/gcn3/3474.gcn3>

Golenetskii, S., et al. 2005c, *GCN Circ.* 3518, <http://gcn.gsfc.nasa.gov/gcn3/3518.gcn3>

Golenetskii, S., et al. 2005d, *GCN Circ.* 3619, <http://gcn.gsfc.nasa.gov/gcn3/3619.gcn3>

Golenetskii, S., et al. 2005e, *GCN Circ.* 4078, <http://gcn.gsfc.nasa.gov/gcn3/4078.gcn3>

Golenetskii, S., et al. 2005f, *GCN Circ.* 4238, <http://gcn.gsfc.nasa.gov/gcn3/4238.gcn3>

Golenetskii, S., et al. 2006a, *GCN Circ.* 4439, <http://gcn.gsfc.nasa.gov/gcn3/4439.gcn3>

Golenetskii, S., et al. 2006b, *GCN Circ.* 4542, <http://gcn.gsfc.nasa.gov/gcn3/4542.gcn3>

Golenetskii, S., et al. 2006c, *GCN Circ.* 4881, <http://gcn.gsfc.nasa.gov/gcn3/4881.gcn3>

Golenetskii, S., et al. 2006d, *GCN Circ.* 5113, <http://gcn.gsfc.nasa.gov/gcn3/5113.gcn3>

Golenetskii, S., et al. 2006e, *GCN Circ.* 5446, <http://gcn.gsfc.nasa.gov/gcn3/5446.gcn3>

Golenetskii, S., et al. 2006f, *GCN Circ.* 5460, <http://gcn.gsfc.nasa.gov/gcn3/5460.gcn3>

Golenetskii, S., et al. 2006g, *GCN Circ.* 5518, <http://gcn.gsfc.nasa.gov/gcn3/5518.gcn3>

Golenetskii, S., et al. 2006h, *GCN Circ.* 5722, <http://gcn.gsfc.nasa.gov/gcn3/5722.gcn3>

Golenetskii, S., et al. 2006i, *GCN Circ.* 5748, <http://gcn.gsfc.nasa.gov/gcn3/5748.gcn3>

Golenetskii, S., et al. 2006j, *GCN Circ.* 5837, <http://gcn.gsfc.nasa.gov/gcn3/5837.gcn3>

Golenetskii, S., et al. 2006k, *GCN Circ.* 5890, <http://gcn.gsfc.nasa.gov/gcn3/5890.gcn3>

Golenetskii, S., et al. 2006l, *GCN Circ.* 5984, <http://gcn.gsfc.nasa.gov/gcn3/5984.gcn3>

Golenetskii, S., et al. 2007a, *GCN Circ.* 6124, <http://gcn.gsfc.nasa.gov/gcn3/6124.gcn3>

Golenetskii, S., et al. 2007b, *GCN Circ.* 6230, <http://gcn.gsfc.nasa.gov/gcn3/6230.gcn3>

Golenetskii, S., et al. 2007c, *GCN Circ.* 6344, <http://gcn.gsfc.nasa.gov/gcn3/6344.gcn3>

Golenetskii, S., et al. 2007d, *GCN Circ.* 6403, <http://gcn.gsfc.nasa.gov/gcn3/6403.gcn3>

Golenetskii, S., et al. 2007e, *GCN Circ.* 6459, <http://gcn.gsfc.nasa.gov/gcn3/6459.gcn3>

- Huang, Y. F., Dai, Z. G., and Lu, T. 2002, *MNRAS*, 332, 735
- Kaneko, Y. et al. 2006, *ApJS*, 166, 298
- Kippen, R. M., Woods, P. M., Heise, J., in’t Zand, J., Briggs, M. S., & Preece, R. D. 2002, in *Gamma-Ray Bursts and Afterglow Astronomy*, eds. G. R. Ricker and R. Vanderspek (New York: AIP), 244
- Lamb, D. Q., Donaghy, T. Q., and Graziani, C. 2005, *ApJ*, 520, 335
- Liang, E., Zhang, B., *ApJ*, 633, 611
- Mészáros, P., Ramirez-Ruiz, E., Rees, M. J., Zhang, B., *ApJ*, 578, 812
- Mochkovitch, R., Daigne, F., Barraud, C., & Atteia, J. L. 2003, in *APS Conf. Ser. 312, Third Rome Workshop on Gamma-Ray Bursts in the Afterglow Era*, ed. M. Feroci et al. (San Francisco: ASP), 381
- Nakagawa, U., et al. 2005, *GCN Circ. 3053*, <http://gcn.gsfc.nasa.gov/gcn3/3053.gcn3>
- Rossi, E., Lazzati, D., and Rees, M. J. 2002, *MNRAS*, 332, 945
- Sakamoto, T., et al. 2004, *ApJ*, 602, 875
- Sakamoto, T., et al. 2005, *ApJ*, 629, 311
- Sakamoto, T., et al. 2006, *ApJ*, 636, L73
- Sakamoto, T., et al. 2008a, *ApJS*, 175, 179
- Sakamoto, T., et al. 2008b, *ApJ*, 679, 570
- Sato, R., et al. 2005, *PASJ*, 57, 1031
- Toma, K., Yamazaki, R., Nakamura, T. 2005, *ApJ*, 635, 481
- Yamazaki, R., Ioka, K., Nakamura, T. 2004, *ApJ*, 607, L103
- Yonetoku, D., et al. 2004, *ApJ*, 609, 935
- Zhang, B. & Mészáros, P. 2002, *ApJ*, 571, 876
- Zhang, B., Dai, X., Lloyd-Ronning, N. M., & Mészáros, P. 2004, 601, L119

Table 1.  $E_{\text{peak}}$  -  $\Gamma$  relation based on the Band function

$\theta$		$E_{\text{peak}} - \Gamma$ relation	1- $\sigma$ lower limit	1- $\sigma$ upper limit
0 (on-axis)	$\log E_{\text{peak}} =$	$3.312 - 0.817\Gamma$	$-29.450 + 57.904\Gamma - 34.337\Gamma^2 + 6.445\Gamma^3$	$-1.073 + 9.840\Gamma - 7.065\Gamma^2 + 1.413\Gamma^3$
15	$\log E_{\text{peak}} =$	$3.184 - 0.793\Gamma$	$-31.986 + 62.511\Gamma - 37.070\Gamma^2 + 6.975\Gamma^3$	$-1.991 + 11.452\Gamma - 7.988\Gamma^2 + 1.587\Gamma^3$
30	$\log E_{\text{peak}} =$	$3.231 - 0.819\Gamma$	$-20.684 + 43.646\Gamma - 26.891\Gamma^2 + 5.185\Gamma^3$	$-6.762 + 19.192\Gamma - 12.065\Gamma^2 + 2.291\Gamma^3$
50	$\log E_{\text{peak}} =$	$3.210 - 0.796\Gamma$	$6.782 - 3.948\Gamma - 0.286\Gamma^2 + 0.348\Gamma^3$	$-6.860 + 18.110\Gamma - 10.740\Gamma^2 + 1.935\Gamma^3$
Weighted	$\log E_{\text{peak}} =$	$3.258 - 0.829\Gamma$	$-20.684 + 43.646\Gamma - 26.891\Gamma^2 + 5.185\Gamma^3$	$-5.198 + 16.568\Gamma - 10.630\Gamma^2 + 2.034\Gamma^3$

Table 2.  $E_{\text{peak}} - \Gamma$  relation based on a CPL model

$\theta$	$E_{\text{peak}} - \Gamma$ relation	1- $\sigma$ lower limit	1- $\sigma$ upper limit
0 (on-axis)	$\log E_{\text{peak}} = 3.722 - 1.033\Gamma$	$1.829 + 1.874\Gamma - 1.638\Gamma^2 + 0.315\Gamma^3$	$-14.504 + 31.357\Gamma - 18.043\Gamma^2 + 3.234\Gamma^3$
15	$\log E_{\text{peak}} = 3.657 - 0.994\Gamma$	$1.829 + 1.874\Gamma - 1.638\Gamma^2 + 0.315\Gamma^3$	$-14.504 + 31.357\Gamma - 18.043\Gamma^2 + 3.234\Gamma^3$
30	$\log E_{\text{peak}} = 3.490 - 0.904\Gamma$	$1.980 + 1.434\Gamma - 1.342\Gamma^2 + 0.258\Gamma^3$	$-8.724 + 20.829\Gamma - 11.819\Gamma^2 + 2.052\Gamma^3$
50	$\log E_{\text{peak}} = 3.664 - 0.984\Gamma$	$-0.742 + 5.847\Gamma - 3.751\Gamma^2 + 0.695\Gamma^3$	$-1.794 + 8.489\Gamma - 4.823\Gamma^2 + 0.813\Gamma^3$
Weighted	$\log E_{\text{peak}} = 3.518 - 0.920\Gamma$	$5.018 - 3.548\Gamma + 1.366\Gamma^2 - 0.229\Gamma^3$	$-9.443 + 22.037\Gamma - 12.478\Gamma^2 + 2.168\Gamma^3$

Table 3: The BAT time-averaged spectral parameters fitted with a simple power-law (PL) model and a power-law times exponential cutoff (CPL) model. See the BAT1 catalog paper for the details about the BAT analysis (Sakamoto et al. 2008a). The degree of freedom in a PL fit and a CPL fit is all 57 and 56 respectively.

GRB	Trigger ID	PL		CPL		
		$\Gamma$	$\chi^2$	$\alpha$	$E_{\text{peak}}$ [keV]	$\chi^2$
GRB 041217	100116	$1.46 \pm 0.07$	74.9	$-0.7 \pm 0.3$	$95^{+27}_{-14}$	54.8
GRB 041224	100703	$1.72 \pm 0.06$	56.1	$-1.1 \pm 0.3$	$74^{+16}_{-9}$	36.7
GRB 050117	102861	$1.50 \pm 0.04$	38.8	$-1.2 \pm 0.2$	$143^{+108}_{-33}$	29.6
GRB 050124	103647	$1.47 \pm 0.08$	58.7	$-0.7 \pm 0.4$	$95^{+39}_{-16}$	45.4
GRB 050128	103906	$1.37 \pm 0.07$	59.3	$-0.7 \pm 0.3$	$113^{+46}_{-19}$	44.8
GRB 050219A	106415	$1.31 \pm 0.06$	103.2	$-0.1 \pm 0.3$	$92^{+12}_{-8}$	45.5
GRB 050219B	106442	$1.53 \pm 0.05$	86.6	$-1.0^{+0.3}_{-0.2}$	$108^{+35}_{-16}$	69.0
GRB 050410	114299	$1.65 \pm 0.08$	78.5	$-0.8 \pm 0.4$	$74^{+19}_{-9}$	61.3
GRB 050416B	114797	$1.4 \pm 0.1$	67.4	$-0.4^{+0.7}_{-0.6}$	$94^{+66}_{-19}$	59.7
GRB 050525A <sup>a</sup>	130088	1.76	166.4	$-1.0 \pm 0.1$	$82^{+4}_{-3}$	17.9
GRB 050716	146227	$1.37 \pm 0.06$	52.5	$-0.8 \pm 0.3$	$123^{+61}_{-24}$	39.4
GRB 050815	150532	$1.8 \pm 0.2$	75.6	$0.9^{+1.9}_{-1.4}$	$44^{+9}_{-6}$	62.1
GRB 050820B	151334	$1.34 \pm 0.04$	89.6	$-0.6 \pm 0.2$	$111^{+21}_{-13}$	48.7
GRB 050915B	155284	$1.90 \pm 0.06$	55.5	$-1.4 \pm 0.3$	$61^{+17}_{-8}$	46.0
GRB 051021B	160672	$1.6 \pm 0.1$	56.9	$-0.6^{+0.8}_{-0.6}$	$72^{+45}_{-13}$	49.7
GRB 060111A	176818	$1.65 \pm 0.07$	69.0	$-0.9 \pm 0.3$	$74^{+19}_{-10}$	50.4
GRB 060115	177408	$1.8 \pm 0.1$	52.6	$-1.0^{+0.6}_{-0.5}$	$63^{+36}_{-11}$	45.8
GRB 060117	177666	$1.93 \pm 0.03$	67.0	$-1.5 \pm 0.1$	$70^{+7}_{-5}$	35.6
GRB 060204B	180241	$1.44 \pm 0.09$	47.0	$-0.8 \pm 0.4$	$100^{+75}_{-21}$	38.9
GRB 060206	180455	$1.71 \pm 0.08$	64.6	$-1.2 \pm 0.3$	$78^{+38}_{-13}$	55.3
GRB 060211A	181126	$1.8 \pm 0.1$	71.5	$-0.9^{+0.6}_{-0.5}$	$58^{+18}_{-8}$	60.6
GRB 060322	202442	$1.58 \pm 0.07$	64.6	$-1.1^{+0.3}_{-0.4}$	$96^{+90}_{-18}$	57.5
GRB 060428B	207399	$2.6 \pm 0.2$	66.7	$-0.8^{+1.6}_{-1.2}$	$22^{+5}_{-13}$	59.1
GRB 060707	217704	$1.7 \pm 0.1$	70.5	$-0.6^{+0.7}_{-0.6}$	$63^{+21}_{-10}$	60.5
GRB 060813	224364	$1.36 \pm 0.04$	54.1	$-1.0 \pm 0.2$	$168^{+117}_{-39}$	43.5
GRB 060825	226382	$1.72 \pm 0.07$	64.7	$-1.2 \pm 0.3$	$73^{+28}_{-11}$	53.7
GRB 060908	228581	$1.35 \pm 0.06$	50.7	$-1.0 \pm 0.3$	$151^{+184}_{-41}$	44.2
GRB 060927	231362	$1.65 \pm 0.08$	70.4	$-0.9 \pm 0.4$	$72^{+25}_{-11}$	57.5
GRB 070420	276321	$1.56 \pm 0.05$	60.7	$-1.2 \pm 0.2$	$120^{+76}_{-24}$	51.1
GRB 070508	278854	$1.35 \pm 0.03$	38.4	$-1.1 \pm 0.1$	$260^{+203}_{-68}$	27.8
GRB 070521	279935	$1.36 \pm 0.04$	57.5	$-1.1 \pm 0.2$	$209^{+234}_{-60}$	50.1

<sup>a</sup>The confidence interval is not calculated because of  $\chi^2_{\nu} > 2$ . Short GRBs, GRB 050820A and GRB 050925 are excluded.

Table 4: The spectral parameters of simultaneously observed by *Konus-Wind* or *HETE-2*.

GRB	Model	$\alpha$	$\beta$	$E_{\text{peak}}$	$\Gamma_{\text{BAT}}$	Reference
GRB 050215B	Band	-	-	$< 35.7^a$	$2.0 \pm 0.2$	Nakagawa et al. (2005)
GRB 050326	Band	$-0.74 \pm 0.09$	$-2.49 \pm 0.16$	$201 \pm 24$	$1.25 \pm 0.04$	Golenetskii et al. (2005a)
GRB 050525A	CPL	$-1.10 \pm 0.05$	-	$84.1 \pm 1.7$	$1.76^c$	Golenetskii et al. (2005b)
GRB 050603	Band	$-0.79 \pm 0.06$	$-2.15 \pm 0.09$	$349 \pm 28$	$1.16 \pm 0.06$	Golenetskii et al. (2005c)
GRB 050713A	CPL	$-1.12 \pm 0.08$	-	$312 \pm 50$	$1.53 \pm 0.08$	Golenetskii et al. (2005d)
GRB 050824	Band	-	-	$< 12.7^b$	$2.8 \pm 0.4$	Crew et al. (2005a)
GRB 050922C	CPL	$-0.83^{+0.26}_{-0.23}$	-	$143 \pm 39$	$1.37 \pm 0.06$	Crew et al. (2005b)
GRB 051008	CPL	$-0.975^{+0.086}_{-0.078}$	-	$886 \pm 157$	$1.13 \pm 0.05$	Golenetskii et al. (2005e)
GRB 051109A	CPL	$-1.25^{+0.59}_{-0.44}$	-	$224 \pm 141$	$1.5 \pm 0.2$	Golenetskii et al. (2005f)
GRB 060105	CPL	$-0.83 \pm 0.03$	-	$424^{+25}_{-22}$	$1.07 \pm 0.04$	Golenetskii et al. (2006a)
GRB 060117	Band	$-1.52^{+0.08}_{-0.07}$	$-2.9^{+0.3}_{-0.5}$	$89 \pm 5$	$1.93 \pm 0.03$	Golenetskii et al. (2006b)
GRB 060313	CPL	$-0.6 \pm 0.2$	-	$922^{+306}_{-177}$	$0.70 \pm 0.07$	Golenetskii et al. (2006c)
GRB 060510	CPL	$-1.66 \pm 0.07$	-	$184^{+36}_{-24}$	$1.57 \pm 0.07$	Golenetskii et al. (2006d)
GRB 060813	Band	$-0.53^{+0.16}_{-0.14}$	$-2.6^{+0.3}_{-0.5}$	$192^{+20}_{-18}$	$1.36 \pm 0.04$	Golenetskii et al. (2006e)
GRB 060814	CPL	$-1.4 \pm 0.2$	-	$257^{+122}_{-58}$	$1.54 \pm 0.03$	Golenetskii et al. (2006f)
GRB 060904A	Band	$-1.0 \pm 0.2$	$-2.6^{+0.4}_{-1.0}$	$163 \pm 31$	$1.55 \pm 0.04$	Golenetskii et al. (2006g)
GRB 061007	Band	$-0.7 \pm 0.4$	$-2.6^{+0.3}_{-0.5}$	$399^{+19}_{-18}$	$1.03 \pm 0.03$	Golenetskii et al. (2006h)
GRB 061021	CPL	$-1.2 \pm 0.1$	-	$777^{+549}_{-237}$	$1.30 \pm 0.06$	Golenetskii et al. (2006i)
GRB 061121	CPL	$-1.32 \pm 0.05$	-	$606^{+90}_{-72}$	$1.41 \pm 0.03$	Golenetskii et al. (2006j)
GRB 061201	CPL	$-0.36^{+0.40}_{-0.65}$	-	$873^{+458}_{-284}$	$0.8 \pm 0.1$	Golenetskii et al. (2006k)
GRB 061222A	Band	$-0.94^{+0.14}_{-0.13}$	$-2.4^{+0.3}_{-1.2}$	$283^{+59}_{-42}$	$1.35 \pm 0.04$	Golenetskii et al. (2006l)
GRB 070220	Band	$-1.2^{+0.3}_{-0.2}$	$-2.0^{+0.3}_{-0.4}$	$299^{+204}_{-130}$	$1.40 \pm 0.04$	Golenetskii et al. (2007a)
GRB 070328	Band	$-1.0 \pm 0.1$	$-2.0^{+0.2}_{-0.4}$	$496^{+172}_{-117}$	$1.24 \pm 0.04$	Golenetskii et al. (2007b)
GRB 070420	CPL	$-1.2 \pm 0.2$	-	$147^{+29}_{-19}$	$1.56 \pm 0.05$	Golenetskii et al. (2007c)
GRB 070508	CPL	$-0.81 \pm 0.07$	-	$188 \pm 8$	$1.36 \pm 0.03$	Golenetskii et al. (2007d)
GRB 070521	CPL	$-0.9 \pm 0.1$	-	$222^{+27}_{-21}$	$1.36 \pm 0.04$	Golenetskii et al. (2007e)

<sup>a</sup>99% upper limit

<sup>b</sup>90% upper limit

<sup>c</sup>The confidence interval is not calculated because of  $\chi^2_\nu > 2$ .

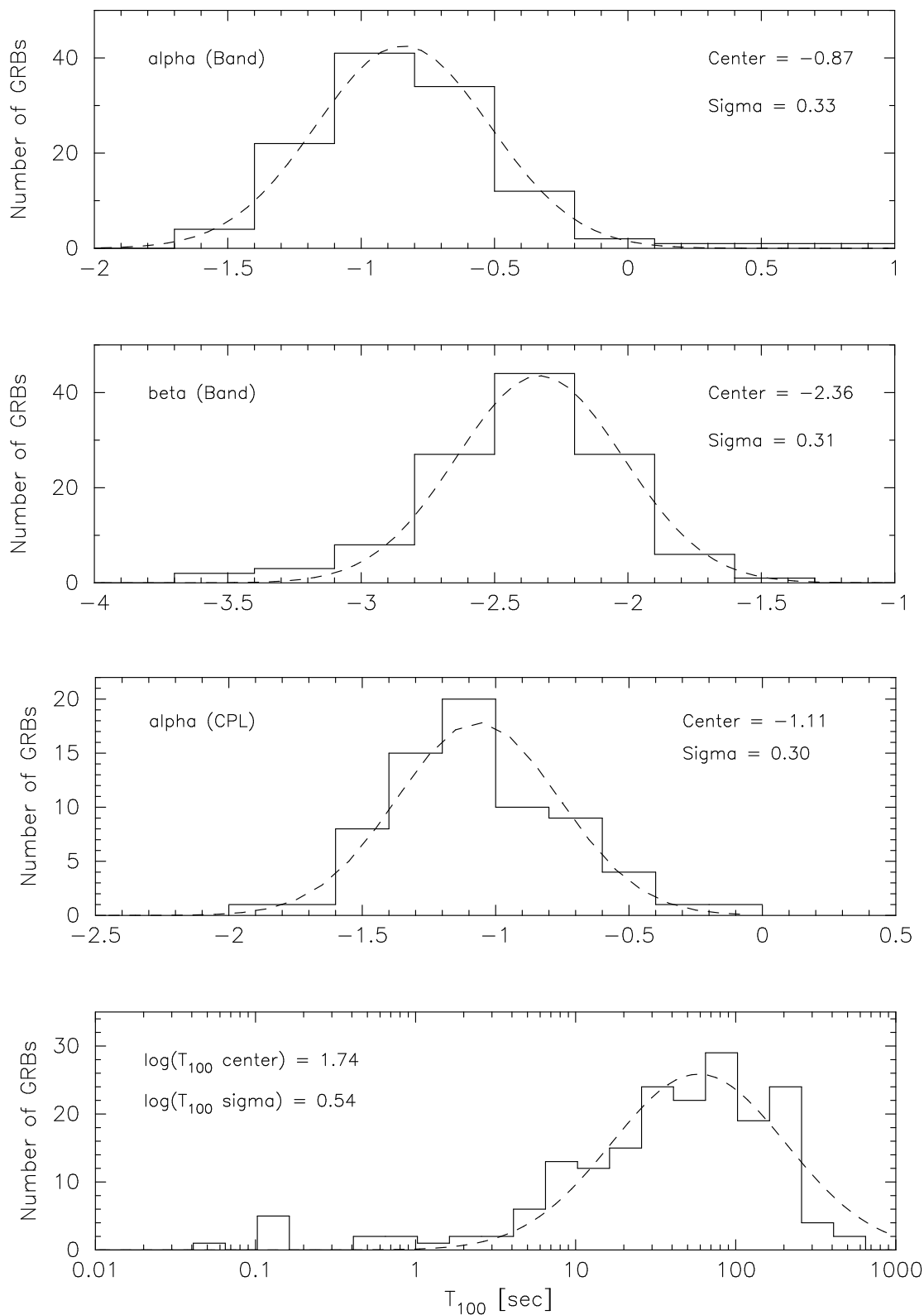


Fig. 1.— Input parameters in the spectral simulations. The distribution of the low energy photon index  $\alpha$ , the high energy photon index  $\beta$  in the Band function, the low energy photon index  $\alpha$  in a CPL model from the BATSE GRB sample, and the BAT  $T_{100}$  duration from top to bottom, respectively. The dotted line represents the best fit in a gaussian.

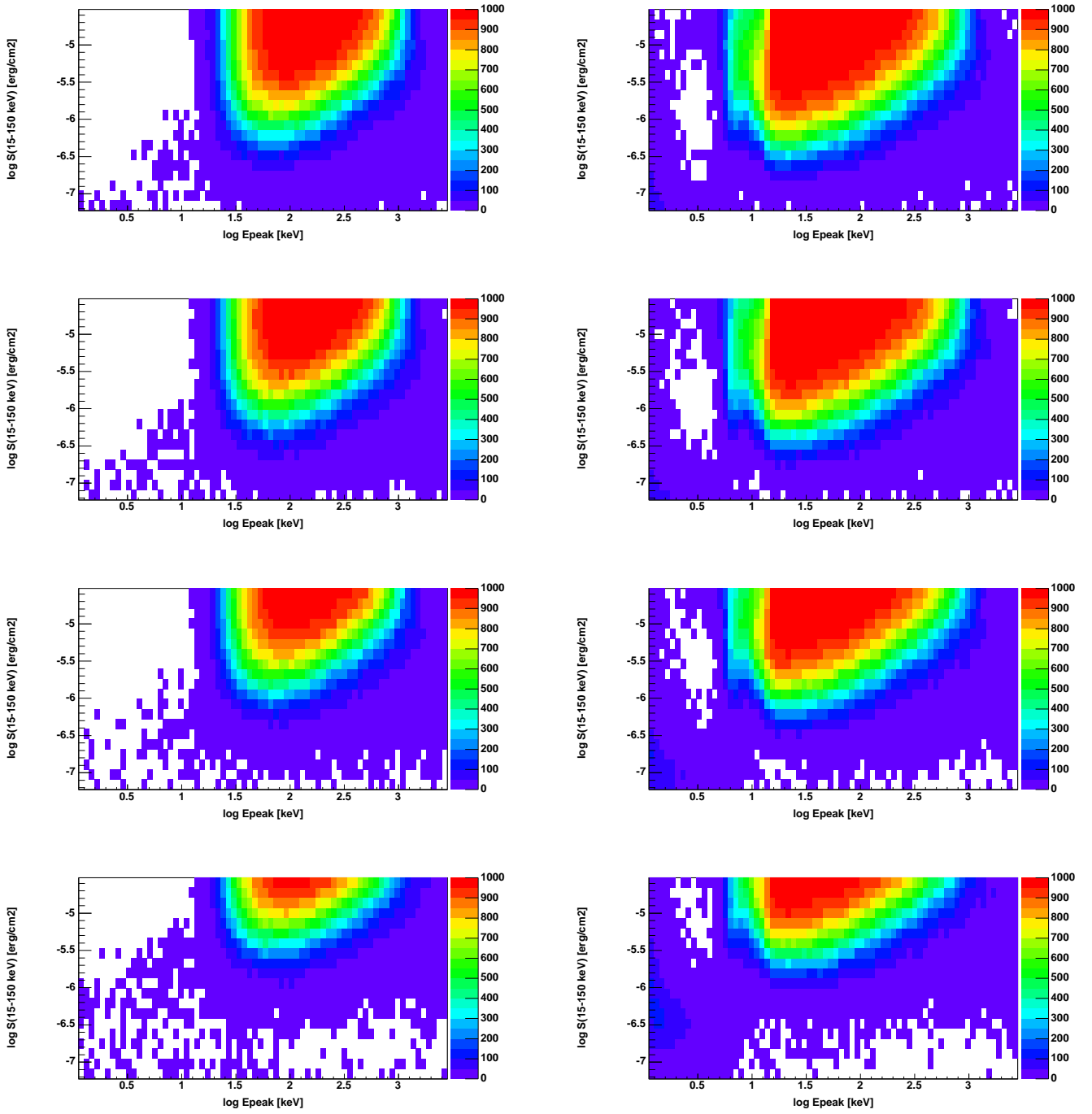


Fig. 2.— The contour maps showing, as a function of the simulated  $E_{\text{peak}}$  and the energy flux in the 15-150 keV band, the number of simulated spectra which have  $\Delta\chi^2 > 6$  (left row for the Band function:  $\Delta\chi^2 \equiv \chi_{\text{PL}}^2 - \chi_{\text{Band}}^2$ ; right row for a CPL model:  $\Delta\chi^2 \equiv \chi_{\text{PL}}^2 - \chi_{\text{CPL}}^2$ ). The incident angles of the simulations are  $0^\circ$ ,  $15^\circ$ ,  $30^\circ$  and  $50^\circ$  from top to bottom.

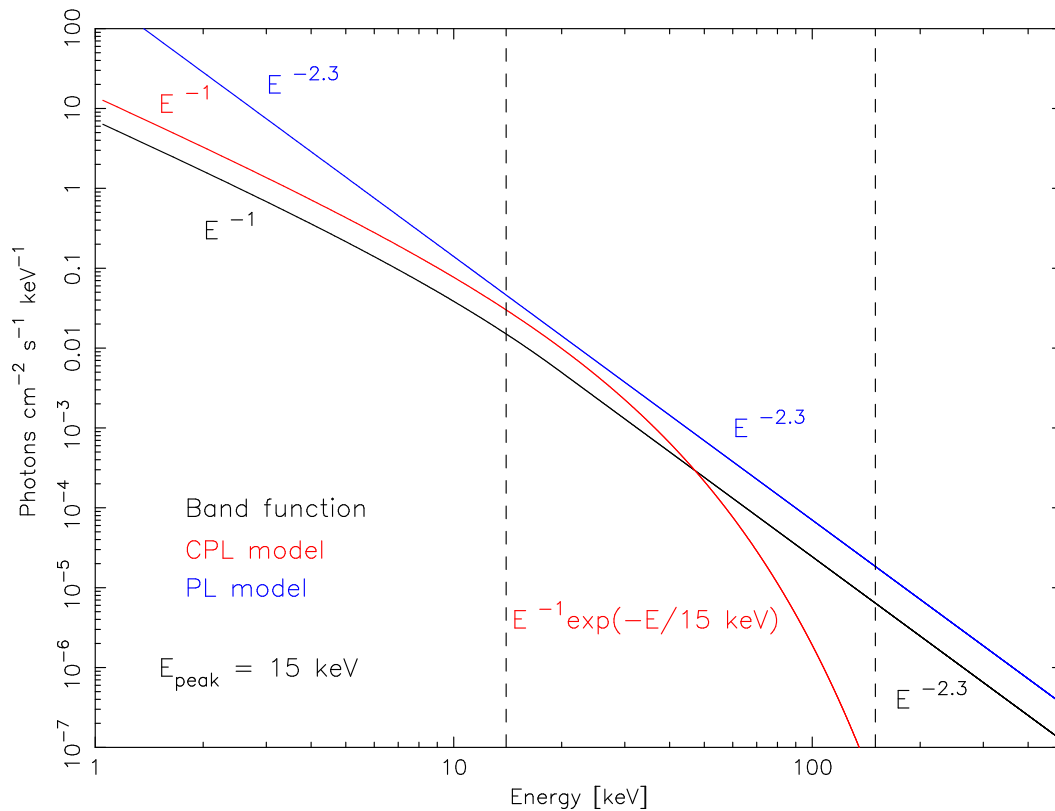


Fig. 3.— The schematic drawing of the photon spectra of the Band function (black) and a CPL model (red) with  $E_{\text{peak}}$  of 15 keV. The low energy photon index is  $-1$  for both models. The high energy photon index of the Band function is  $-2.3$ . A PL model with a photon index of  $-2.3$  is also overlaid in the plot (blue). The vertical dotted lines are the BAT observed energy band of 15-150 keV.

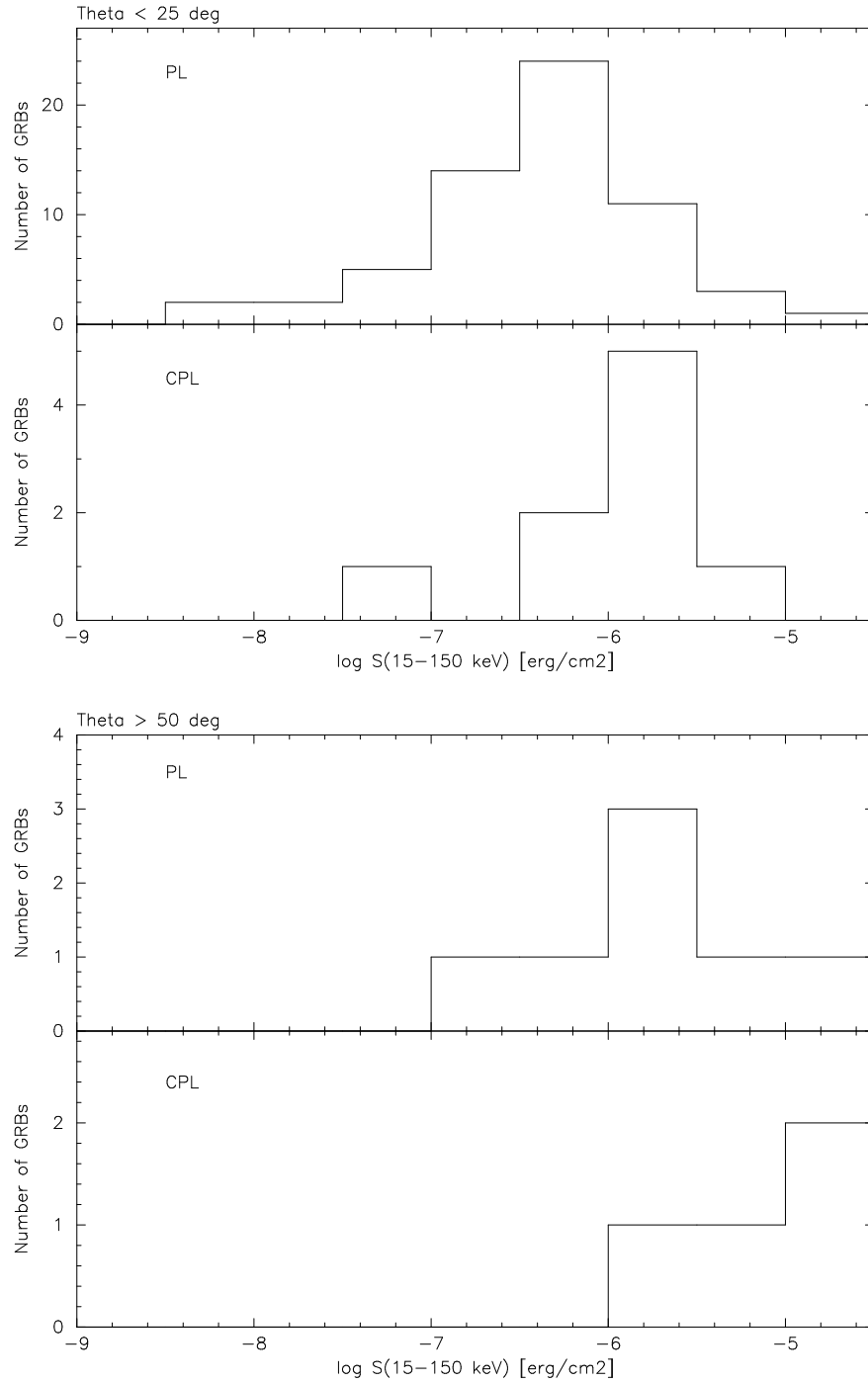


Fig. 4.— The number of GRBs acceptably fit by a PL model (top panel) and by a CPL model (bottom panel) as a function of the fluence in the 15-150 keV band. The samples of the incident angles of bursts less than 25 degrees (top) and larger than 50 degrees (bottom).

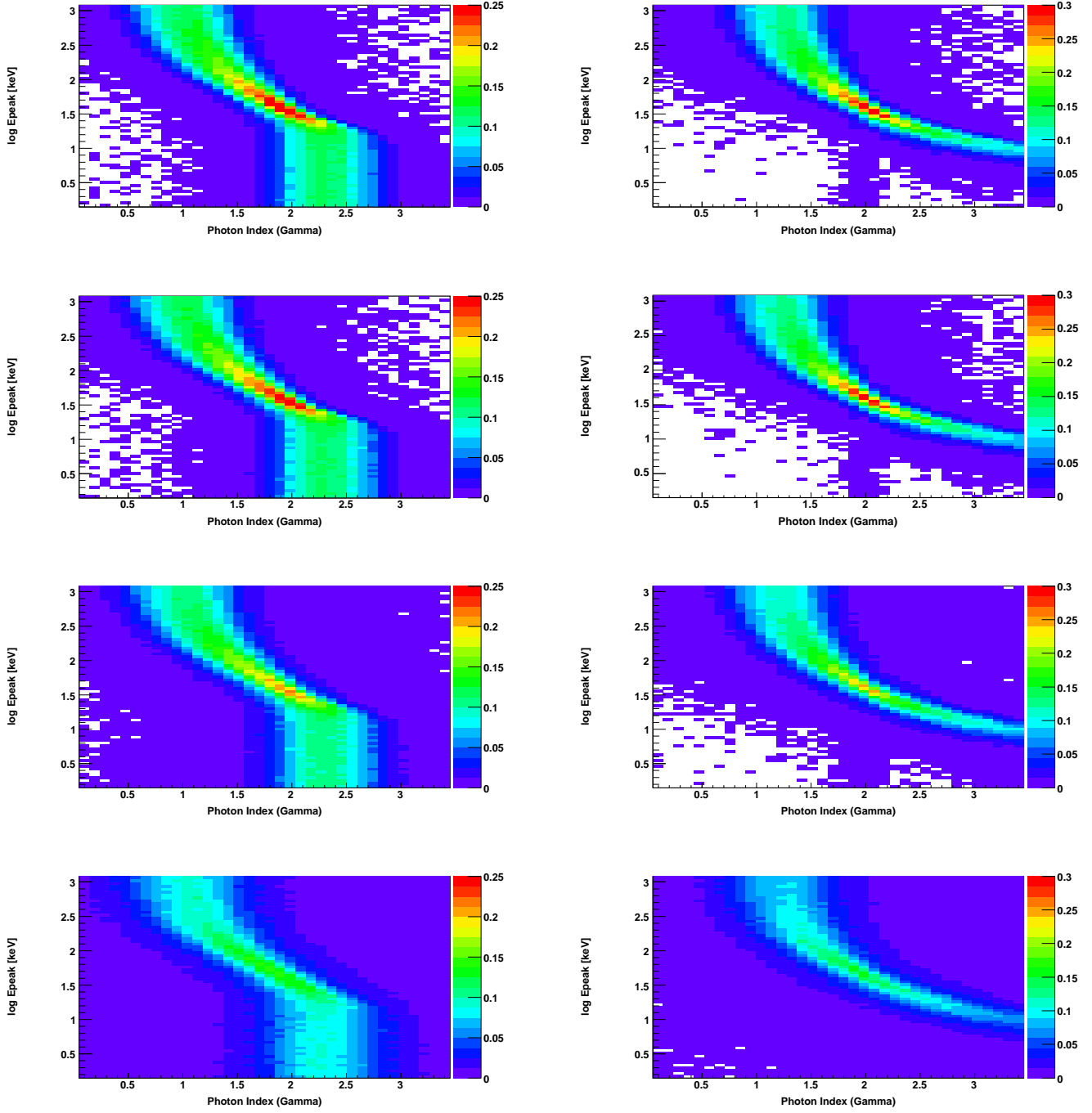


Fig. 5.— Contour maps showing the number of simulated spectra as a function of photon index and input  $E_{\text{peak}}$ . The left and right rows are the Band function and a CPL model, respectively. The incident angles of the simulations are  $0^\circ$ ,  $15^\circ$ ,  $30^\circ$ , and  $50^\circ$  from top to bottom.

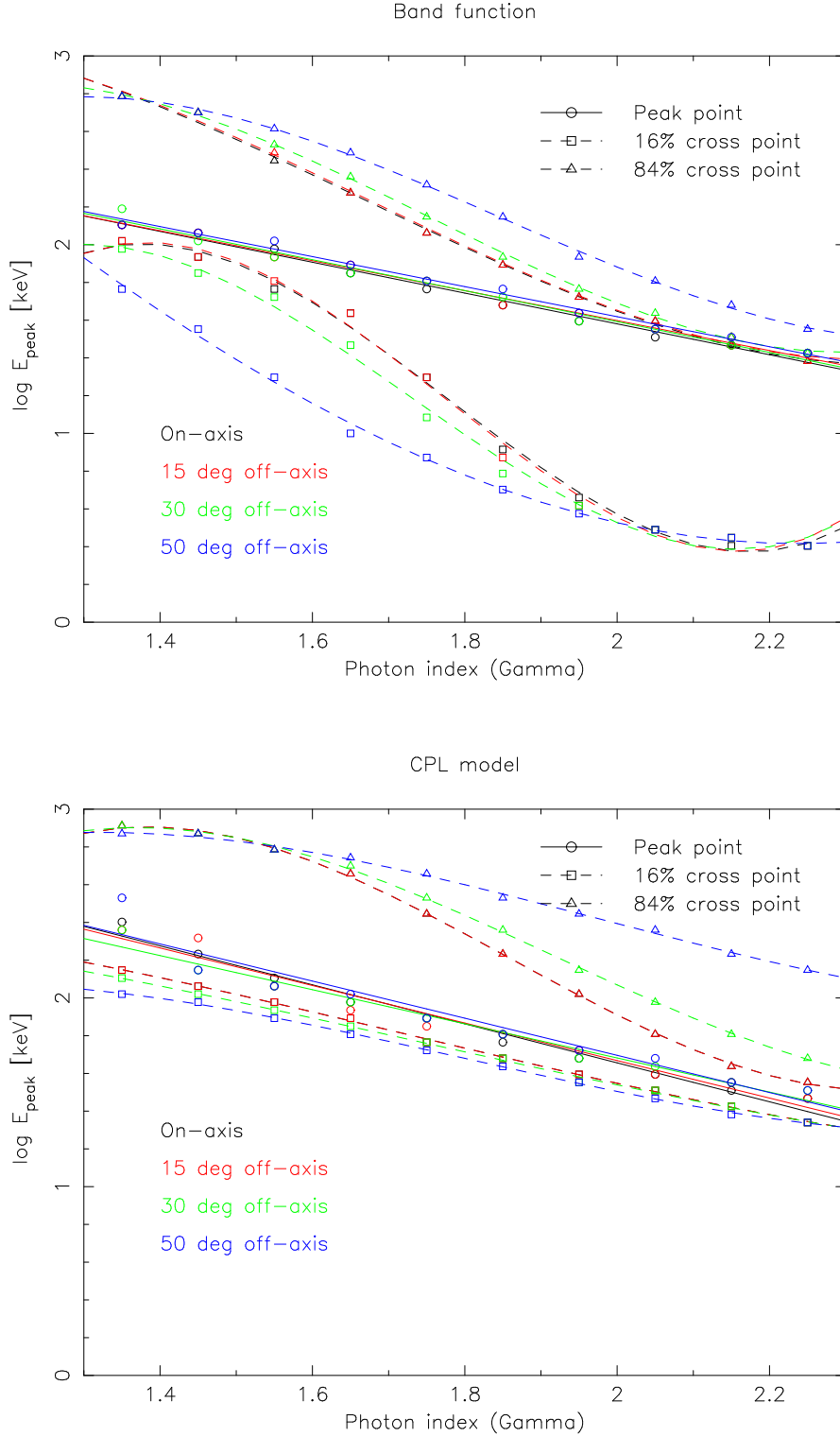


Fig. 6.— The best fit  $E_{\text{peak}} - \Gamma$  relations (solid line) and the lower and higher  $1-\sigma$  confidence level of the relations (dashed lines) for the Band function (top) and a CPL model (bottom) with the data points (circles:  $E_{\text{peak}}$  at the peak of the histogram of  $\Gamma$ , squares:  $E_{\text{peak}}$  value of 16% crossing point of the histogram of  $\Gamma$ , and triangles:  $E_{\text{peak}}$  value of 84% crossing point of the histogram of  $\Gamma$ ). The black, red, green and blue show the cases of incident angles  $0^\circ$ ,  $15^\circ$ ,  $30^\circ$  and  $50^\circ$ , respectively.

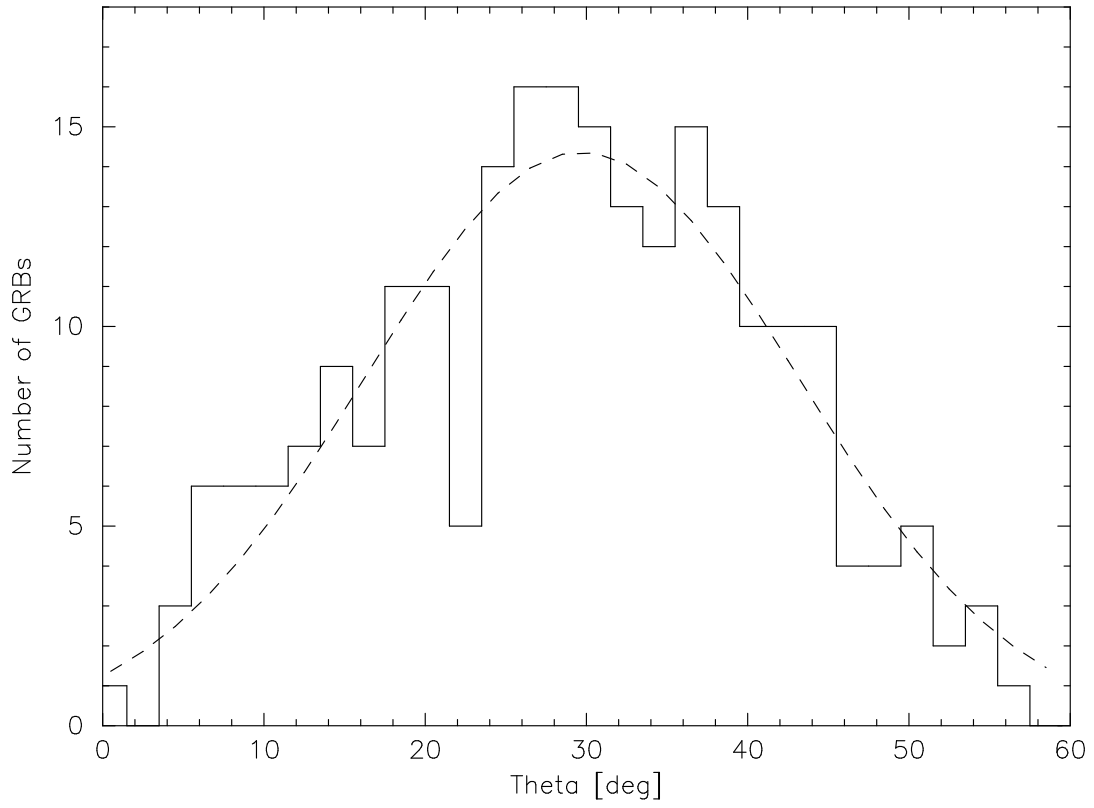


Fig. 7.— The incident angle ( $\theta$ ) distribution of the BAT GRBs. The dotted line is the best fit gaussian model.

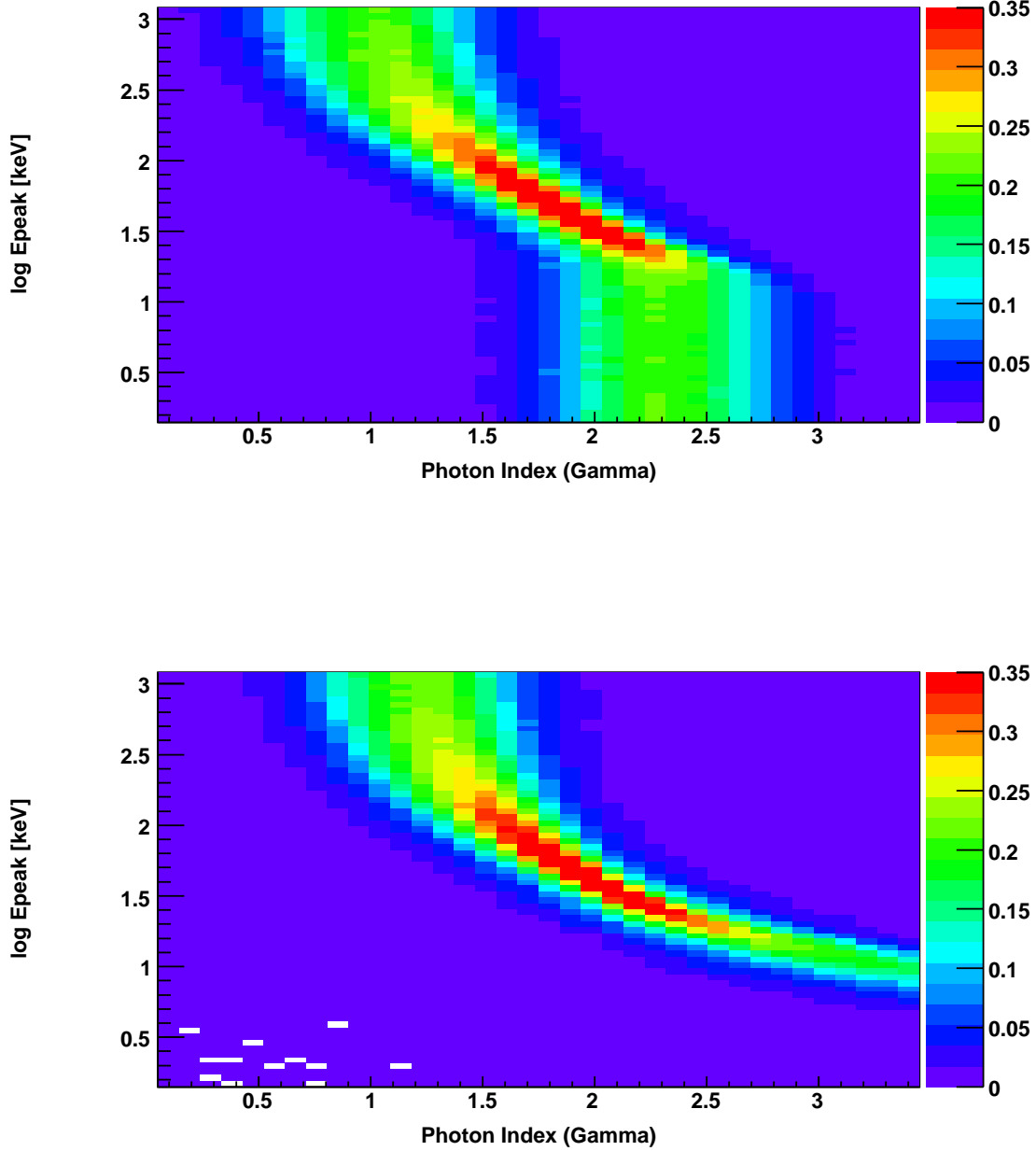


Fig. 8.— Contour maps showing the number of simulated spectra as a function of photon index and input  $E_{\text{peak}}$  after weighting the simulation results of  $0^\circ$ ,  $15^\circ$ ,  $30^\circ$ , and  $50^\circ$  incident angles by the incident angle distribution of the BAT GRBs shown in Figure 7 (top: the Band function and bottom: a CPL model).

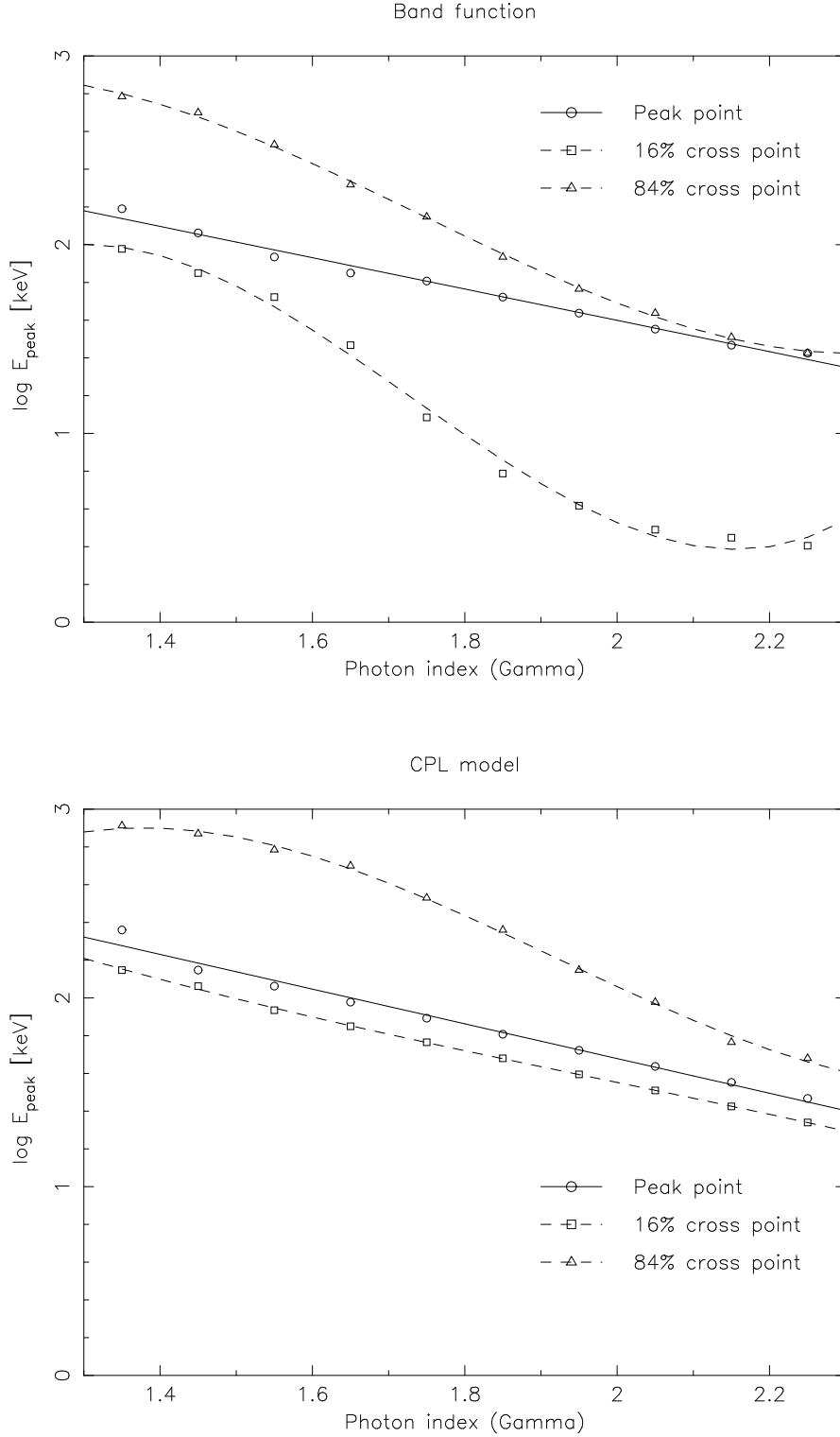


Fig. 9.— The best fit weighted  $E_{\text{peak}} - \Gamma$  relations by the incident angles (solid line) and the lower and higher  $1-\sigma$  confidence level of the relations (dashed lines) for the Band function (top) and a CPL model (bottom) with the data points (circles:  $E_{\text{peak}}$  at the peak of the histogram of  $\Gamma$ , squares:  $E_{\text{peak}}$  value of 16% crossing point of the histogram of  $\Gamma$ , and triangles:  $E_{\text{peak}}$  value of 84% crossing point of the histogram of  $\Gamma$ ).

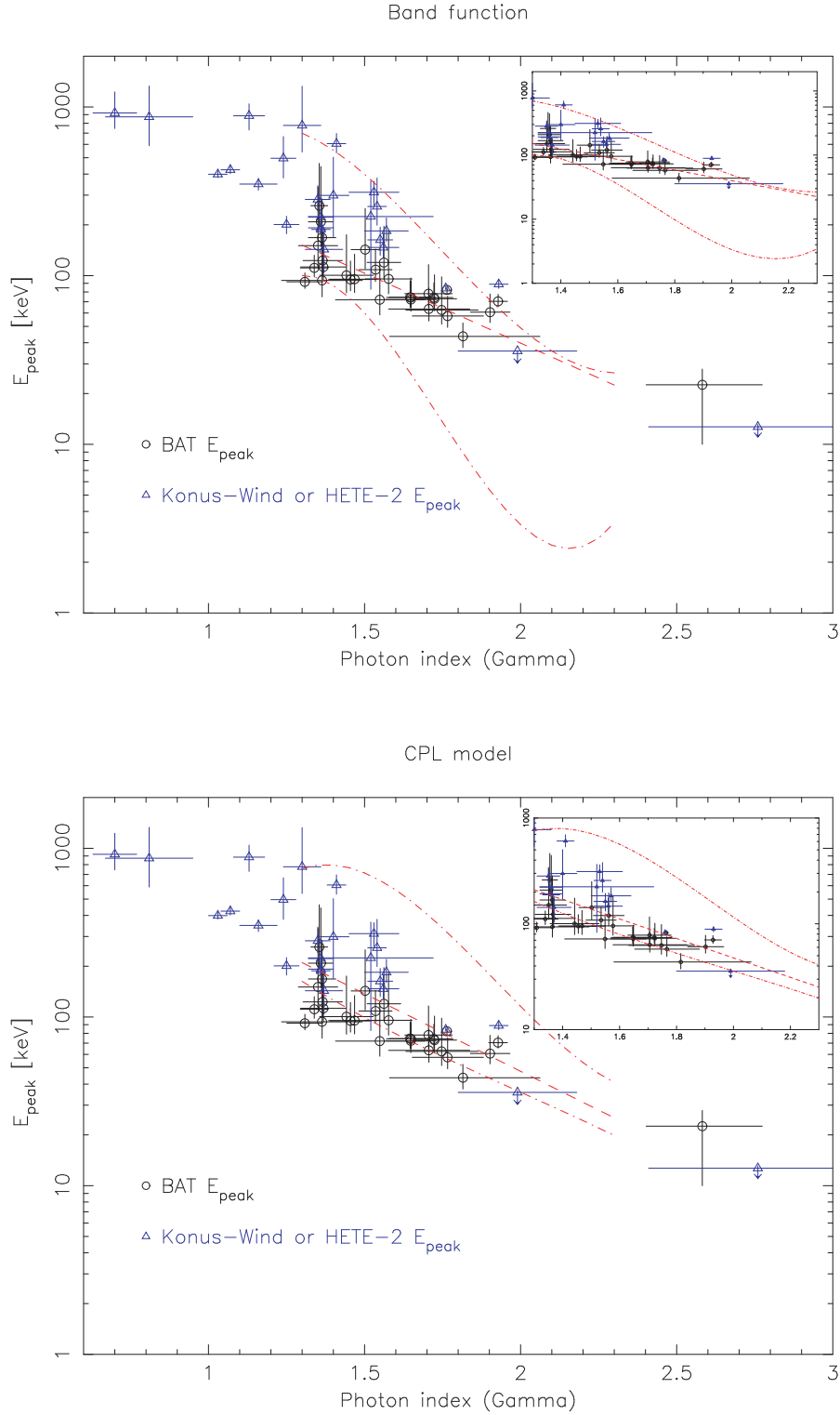


Fig. 10.— The distribution of  $E_{\text{peak}}$  and photon index,  $\Gamma$ , in a PL fit in the BAT GRB sample (black circles). The GRBs which were simultaneously observed by *HETE-2* and *Konus-Wind* are overlaid (blue triangles). The weighted  $E_{\text{peak}}$  -  $\Gamma$  relation for the Band function (top) and a CPL model (bottom) with 1- $\sigma$  confidence level is overlaid on the data. *Inset*: The extended figures of  $\Gamma$  from 1.3 to 2.3 where the  $E_{\text{peak}}$  -  $\Gamma$  relation is valid.

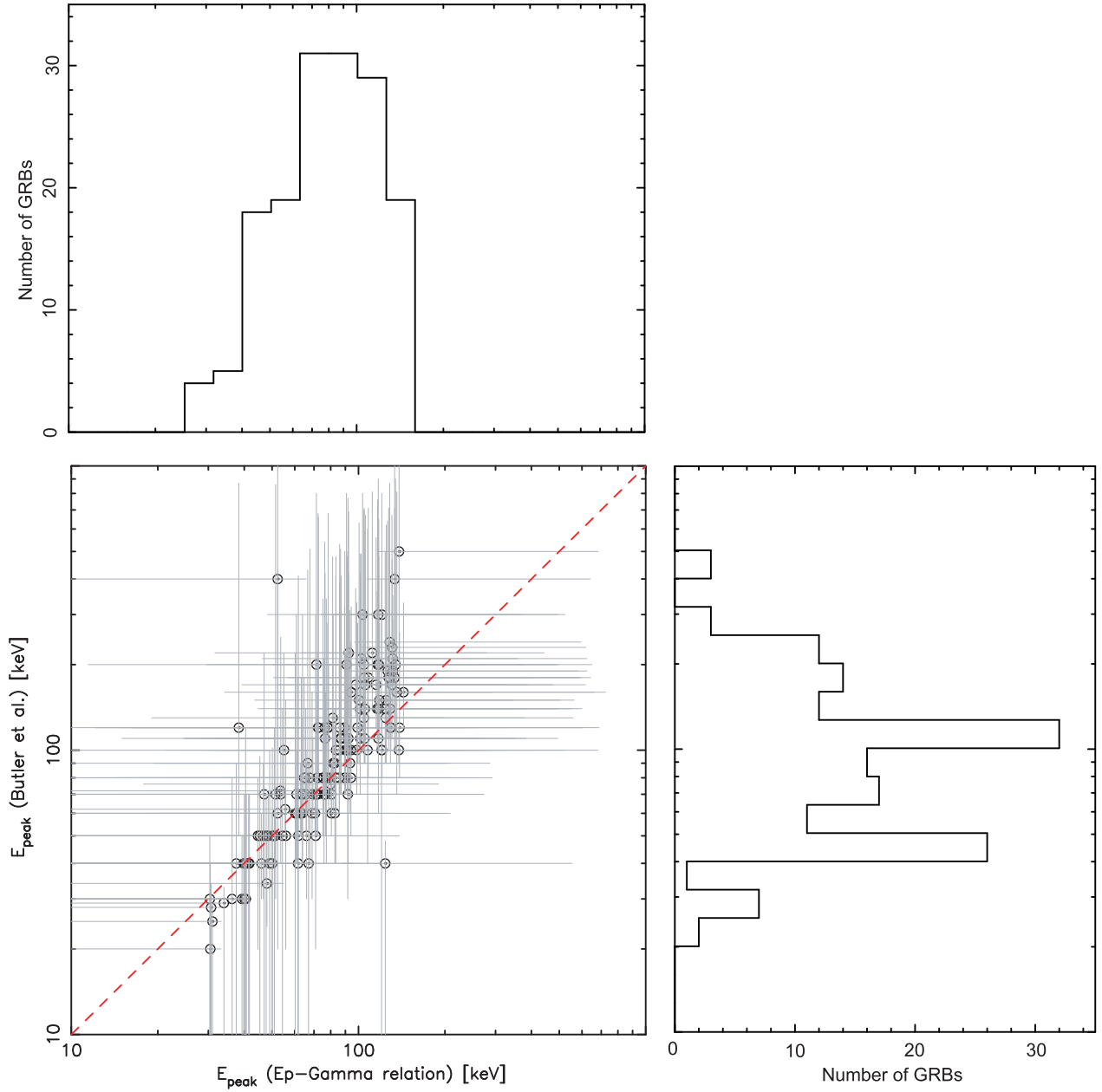


Fig. 11.— The relationship between  $E_{\text{peak}}$  reported by Butler et al. (2007) and  $E_{\text{peak}}$  derived from the weighted  $E_{\text{peak}} - \Gamma$  relation for the Band function. The sample only contains long bursts which have a PL photon index  $\Gamma$  from 1.3 to 2.3. Both  $E_{\text{peak}}$  distributions of Butler et al. (2007) and the  $E_{\text{peak}} - \Gamma$  relation for the same sample are shown in the histograms.